A High-Avidity T-cell Receptor Redirects Natural Killer T-cell Specificity and Outcompetes the Endogenous Invariant T-cell Receptor

Elisa Landoni[1], Christof C. Smith[1,2], Giovanni Fucá[1], Yuhui Chen[1], Chuang Sun[1], Benjamin G. Vincent[1,2,3,4], Leonid S. Metelitsa[5], Gianpietro Dotti[1,2], and Barbara Savoldo[1,6]

ABSTRACT

T-cell receptor (TCR) gene transfer redirects T cells to target intracellular antigens. However, the potential autoreactivity generated by TCR mispairing and occurrence of graft-versus-host disease in the allogenic setting due to the retention of native TCRs remain major concerns. Natural killer T cells (NKT) have shown promise as a platform for adoptive T-cell therapy in cancer patients. Here, we showed their utility for TCR gene transfer. We successfully engineered and expanded NKTs expressing a functional TCR (TCR NKTs), showing HLA-restricted antitumor activity in xenogeneic mouse models in the absence of graft-versus-mouse reactions. We found that TCR NKTs downregulated the invariant TCR (iTCR), leading to $iTCR^{+}TCR^{+}$ and $iTCR^{-}TCR^{+}$ populations. In-depth analyses of these subsets revealed that in $iTCR^{-}TCR^{+}$ NKTs, the iTCR, although expressed at the mRNA and protein levels, was retained in the cytoplasm. This effect resulted from a competition for binding to CD3 molecules for cell-surface expression by the transgenic TCR. Overall, our results highlight the feasibility and advantages of using NKTs for TCR expression for adoptive cell immunotherapies. NKT-low intrinsic alloreactivity that associated with the observed iTCR displacement by the engineered TCR represents ideal characteristics for "off-the-shelf" products without further TCR gene editing.

Introduction

The role played by cytotoxic T cells in tumor control has been recognized for years (1), but the clinical utility of their adoptive transfer has remained elusive due to the low frequency of high-avidity, tumor-specific T cells naturally circulating in peripheral blood (2). Advances in gene engineering have facilitated the introduction of tumor-antigen specificity in polyclonal T cells via expression of ectopic T-cell receptors (TCR; ref. 3). Using this strategy, clinically relevant numbers of TCR-redirected T cells for adoptive transfer can be generated and have produced encouraging clinical results (4, 5).

Despite the clinical success, a major issue of the TCR technology remains the expression of both the ectopic and endogenous TCR chains within the same T cell. This phenomenon can cause competition for binding to CD3 molecules, resulting in a reduced expression of the transgenic TCR (6) and TCR mispairing between the endogenous and transgenic TCR chains, causing potential autoreactivity (7). The retention of functional endogenous TCRs may exacerbate graft-versus-host disease (GvHD) if these cells are used as an allogeneic product (8).

Several strategies have been developed to enhance TCR transgenic expression, such as the inclusion of a codon-optimized sequence (9), the addition of extra disulfide bonds to the transgenic TCR chains (10), the introduction of murine residues in the TCR constant region domain (11), and the replacement of key amino acids in the framework of the variable region (3, 12). siRNA gene silencing (13) and TCR gene editing (14) have been explored to knockdown the endogenous receptor of T cells for replacement with a tumor-specific TCR. However, siRNA-mediated TCR knockdown is generally suboptimal, and the scale-up of gene editing for clinical use remains challenging and of unknown safety profile.

We thus have explored the use of natural killer T cells (NKT) as a TCR-based cell platform to overcome the issues associated with TCR engineering in T cells. Type 1 NKTs are an evolutionarily conserved subset of innate lymphocytes characterized by expression of the invariant TCR α-chain Vα24-Jα18 and reactivity to glycolipids presented by the monomorphic MHC class I–like molecule CD1d (15). In humans, the invariant TCR (iTCR) Vα24-Jα18 chain is paired almost exclusively with TCR Vβ11 (TRBV25-1) chains (16). We reasoned that the limited repertoire of the iTCR and its CD1d restriction should minimize, if not eliminate, both the TCR mispairing phenomena and the risk of GvHD when NKTs express a tumor-specific TCR. Here, we showed the successful TCR engineering, expansion, and HLA-restricted antitumor activity of TCR-redirected NKTs, and we dissected the mechanism by which the transgenic TCR displaces the endogenous iTCR from the cell surface of engineered NKTs.

Materials and Methods

Cell lines

The tumor cell lines SK-MEL-5 and M14 (melanoma), T2 (TAP transporter deficient), SupT1 ($CD3^{+}TCR^{-}$), and 293T cells were obtained from the ATCC between 2015 and 2018. The tumor cell

[1]Lineberger Comprehensive Cancer Center, University of North Carolina at Chapel Hill, Chapel Hill, North Carolina. [2]Department of Microbiology and Immunology, University of North Carolina at Chapel Hill, Chapel Hill, North Carolina. [3]Department of Medicine, Division of Hematology/Oncology, Lineberger Comprehensive Cancer Center, University of North Carolina at Chapel Hill, Chapel Hill, North Carolina. [4]Curriculum in Bioinformatics and Computational Biology, University of North Carolina at Chapel Hill, Chapel Hill, North Carolina. [5]Department of Pediatrics, Baylor College of Medicine, Houston, Texas. [6]Department of Pediatrics, University of North Carolina at Chapel Hill, Chapel Hill, North Carolina.

Note: Supplementary data for this article are available at Cancer Immunology Research Online (http://cancerimmunolres.aacrjournals.org/).

Corresponding Author: Barbara Savoldo, University of North Carolina at Chapel Hill, 125 Mason Farm Road, Marsico Hall 5203, Chapel Hill, NC 27599-7290. Phone: 919-962-8414; Fax: 919-843-9107; E-mail: bsavoldo@med.unc.edu

Cancer Immunol Res 2020;8:57–69

doi: 10.1158/2326-6066.CIR-19-0134

line C8161 (melanoma) was obtained in 2016 from the tissue culture facility at University of North Carolina, Chapel Hill (TCF, UNC-CH). K562 cells were previously established as described by Quintarelli and colleagues (17). All cells were maintained in culture with the appropriate media, either RPMI-1640 (Gibco), DMEM (Gibco), or IMDM (Gibco) supplemented with 10% FBS (Sigma), 1% L-glutamine (Gibco), and 1% penicillin–streptomycin (Gibco) in a humidified atmosphere containing 5% CO_2 at 37°C. The M14 cell line was transduced with an SFG gamma retroviral vector encoding the HLA-A2*0201 molecule (17) to obtain the M14-A2 cell line upon cell sorting. SK-MEL-5, M14-wild-type (wt), and M14-A2 cells were transduced with an SFG gamma retroviral vector encoding the firefly luciferase gene and the fusion protein enhanced GFP (eGFP-FFluc; ref. 18). Cells were kept in culture for less than 6 consecutive months, after which aliquots from the original expanded vial were used. All tumor cell lines were routinely tested to exclude contamination with *Mycoplasma* and assessed for the expression of transgenes (such as HLA-A2, CD40L, CD80, OX40L, and eGFP) and tumor markers by flow cytometry to confirm identity.

Retroviral constructs and generation of retroviral supernatants

Retroviral supernatants were prepared by transient transfection of 293T cells (17) and used to transduce T cells and NKTs (isolated as stated below). The HLA-A2–restricted TCRs specific for Tyrosinase$_{368\text{-}376}$ (Tyr-TCR recognizing the YMDGTMSQV peptide) and MART-1$_{26\text{-}35}$ (MART-1-TCR recognizing the ELAGIGILTV peptide) were obtained from Frankel and colleagues (19) and were cloned into the SFG retroviral vector (20). The HLA-A2–restricted survivin-specific TCR (Sur-TCR recognizing the LMLGEFLKL peptides 96–104) and the HLA-A2–restricted PRAME-specific TCR (PRAME-TCR recognizing the ALYVDSLFFL peptide p300) are previously described (21). The human CD8α cDNA (NM_001768) was cloned into the SFG retroviral vector. The human CD3 complex (CD3δ-2A-CD3γ-2A-CD3ε-2A-CD3ζ) was designed as previously reported (6) and synthetized from Geneart and cloned in the SFG retroviral vector.

NKT and T-cell isolation, transduction, and *in vitro* expansion

Buffy coats from healthy volunteer blood donors were purchased from the Gulf Coast Regional Blood Center (Houston, TX). Peripheral blood mononuclear cells (PBMC) were isolated by Lymphoprep (Accurate Chemical and Scientific Corporation) density gradient centrifugation, according to the manufacturer's protocol. NKTs were purified from PBMCs using anti-iNKT microbeads (Miltenyi Biotech). NKTs were cultured in complete medium, consisting of 45% Click's medium (Irvine Scientific), 45% RPMI-1640 (Hyclone), 10% FBS (Hyclone), 1% L-glutammine (Gibco), and 1% penicillin–streptomycin (Gibco). Upon NKT-positive selection (LS column, Miltenyi Biotech), the negative fraction was used as feeder cells after irradiation (40 Gy, RS-2000 Biological System). For the first stimulation (S1), feeder cells were used once at day 0 at the PBMC:NKT ratio of 10:1. α-Galactosylceramide (αGalCer, 100 ng/mL, Diagnocine LLC) was added at day 0 and IL2 (200 IU/mL, STEMCELL Technologies) was added at days 0, 2, and 4. NKTs were transduced in retronectin (Takara, 7 μg/mL) 24-well coated plates (22) at day 6 when the NKT purity was more than 85%, and cells were restimulated with irradiated feeder cells, at the PBMC:NKT ratio of 5:1 (S2). The feeder cells were loaded with the peptide specific for each TCR (20 μmol/L, YMDGTMSQV for the Tyr-TCR, ELAGIGILTV for the MART-1-TCR, or ALYVDSLFFL for the PRAME-TCR from Genemed Synthesis) and αGalCer (100 ng/mL) in the presence of IL2 (200 IU/mL). NKTs were then further expanded for 10 days in the presence of IL2 (200 IU/mL). In selected experiments, NKTs, $CD8^+$, and unselected T cells were isolated from the same buffy coat. T cells were positively (LS column, Miltenyi Biotech) selected using CD8-specific microbeads (Miltenyi Biotech). Unselected T cells and $CD8^+$ T cells were activated, transduced, and expanded in complete medium with IL7 (10 ng/mL, PeproTech) and IL15 (5 ng/mL, PeproTech) as previously reported (23). Briefly, T cells were activated on anti-CD3 (1 μg/mL, Miltenyi Biotech) and anti-CD28 (1 μg/mL, BD Biosciences) 24-well coated plates. At day 2, T cells were transduced in retronectin (7 μg/mL) 24-well coated plates. On day 10, T cells were stimulated with peptide-loaded (20 μmol/L) and irradiated (80 Gy) artificial antigen-presenting cells (aAPC) consisting of K562 cells expressing CD40L, CD80, OX40L, and the HLA-A*02 molecules (17) at an aAPC:T-cell ratio of 1:4, and further expanded using IL7 (10 ng/mL) and IL15 (5 ng/mL) for 10 days. In selected experiments, NKTs were cotransduced with retroviral vectors encoding the CD8α or the CD3 complex.

Immunophenotyping and flow sorting

T and NKT cells were stained with antibodies (Ab) against CD3 (APC-H7, clone SK7), CD62L (BV605, clone DREG-56), PD-1 (PE-Cy7, clone EH12.1), LAG3 (PE, clone T47-530), TIM3 (BV711, clone 7D3), CD45 (APC, clone 2D1), CD4 (PE-Cy7, clone SK3), and CD8 (Alexa Fluor 700, clone RPA-T8) from BD Biosciences. Tumor cells and aAPCs were stained with Abs against HLA-A2 (PE, clone BB7.2) and CD276 (BV421, clone 7-517) from BD Biosciences. The purity of NKTs was assessed by staining the cells with a tetramer specific for the iTCR (PE-conjugated human CD1d tetramer loaded with αGalCer; ProImmune) and the PE-conjugated Ab specific for TCR Vα24 chain (anti-iNKT, clone 6B11, from BD Biosciences). The expression of the Tyr-TCR in NKTs was assessed using a Tyr-TCR-specific pentamer (Pro5 MHC Pentamer A*02:01 YMDGTMSQV; ProImmune) followed by the staining with the Pro5 Fluorotag APC (ProImmune). NKT transduction efficiency with ectopic TCRs was assessed with an FITC-conjugated Ab specific for the TCR β12 chain (for the Tyr-TCR and MART-1-TCR; Beckman Coulter) or the TCR β14 chain (for the PRAME-TCR; Beckman Coulter), or stained with an APC-conjugated Ab specific for the murine TCR constant β chain (for the Sur-TCR; BD Biosciences). Data acquisition was performed on a BD FACSCanto II or BD LSRFortessa using the BD FACS-Diva software. Data analyses were performed with the FlowJo software. To count the number of CD3 and iTCR molecules expressed from NKTs, we used the PE Fluorescence Quantitation Kit (BD Quantibrite). In selected experiments, NKTs were costained with an anti-iTCR tetramer and anti-Tyr-TCR pentamer, and the $iTCR^+$Tyr-TCR^-, $iTCR^-$Tyr-TCR^+, and $iTCR^+$Tyr-TCR^+ NKTs were sorted using a FACSAria II at the Flow Cytometry Core Facility (UNC, Chapel Hill). After sorting, cells (purity >96%) were kept in culture overnight in complete media and IL2 (200 IU/mL) before performing the functional assays.

^{51}Cr-release assay

The cytotoxic activity of NKTs and $CD8^+$ T cells was evaluated using a standard 5-hour ^{51}Cr release assay (17). In brief, 5×10^3 ^{51}Cr (PerkinElmer)-labeled target cells [$HLA\text{-}A2^+$ mismatched phytohemagglutinin (PHA) blasts; ref. 24; M14-wt, M14-A2, C8161, and SK-MEL-5) per well were plated in triplicate in a 96-well plate (v bottom) with different ratios (40:1, 20:1, 10:1, and 5:1) of effector cells and incubated for 5 hours at 37°C. The supernatant was collected and analyzed with a gamma-counter (PerkinElmer). $HLA\text{-}A2^+$ (PHA) blasts were incubated for 2 hours at 37°C with specific peptides (100 nmol/L, YMDGTMSQV for the Tyr-TCR or ELAGIGILTV for the MART-1-TCR) and washed twice with complete medium. Target cells

were incubated with medium alone or in 1% Triton X-100 (Sigma-Aldrich) to determine the spontaneous and maximum ^{51}Cr release, respectively. The mean percentage of specific lysis of triplicate wells was calculated as follows: [(test counts − spontaneous counts)/(maximum counts − spontaneous counts)] × 100%.

Confocal microscopy

SupT1 cells and NKTs were prepared according to the manufacturer's instructions (Abcam immunofluorescence protocol). Briefly, cells were fixed with cytofix buffer (BD Biosciences) and permeabilized with 0.1% Triron X in PBS. Cells were then incubated with anti-Vα24Jα18 (clone 6B11, Novus Biologicals) diluted at 1:800 in PBS/1% BSA. The Alexa Fluor 546 goat anti-mouse IgG1 (Invitrogen) diluted at 1:500 in PBS/1% BSA was used as a secondary Ab. Cells were mounted cover slips with one drop of ProLong Diamond Antifade Mountant with DAPI (Invitrogen). Data acquisition was performed on LSM700 Zeiss confocal microscopy using ZEN software (ZEISS Microscopy). Data analysis was performed with Fiji software.

TCR repertoire profiling/TCR amplicon sequencing

DNA or RNA were extracted from sorted NKTs using the Qiagen DNeasy or RNeasy micro kits. NKT receptor β chain libraries were prepared using the Clontech SMARTer Human TCR α/β profiling kit, according to the manufacturer's protocol. Libraries were sequenced via 2 × 150 paired end on an Illumina MiSeq at the UNC High-Throughput Sequencing Facility. TCR variable chain calling was performed using IMGT/HighV-QUEST, with subsequent analyses performed using the tcR R package (25).

Real-time qPCR

iTCR and Tyr-TCR expression and integration were measured in NKTs by qPCR with specific primers and probes and normalized to the 18S gene expression. Briefly, RNA was extracted from NKTs (RNeasy Plus Kit, Qiagen), and 1 μg of RNA was used for reverse transcription (5X VILO Reaction Mix and 10X SuperScript Enzyme Mix from Invitrogen). For the qPCR reaction (TaqMan 2X Universal PCR Master Mix from Life Technologies), 20 ng of cDNA were ran in duplicates. The relative expression was calculated as follows: $2^{-\,[(CTgene\ -\ CT18S)\ -\ CTV\alpha24\ in\ NT\text{-}NKTs]}$. DNA was extracted from NKTs (DNeasy Blood and Tissue Kit, Qiagen) and 500 ng of DNA was used for the qPCR reaction. To calculate the number of copies of Tyr-TCR construct in NKTs post sorting, we created a standard curve with the SFG Tyr-TCR plasmid and the QuantStudio Real-Time PCR software automatically calculated the number of copies/100 ng DNA. Data acquisition was performed on a QuantStudio 6 Flex from Life Technologies using the QuantStudio Real-Time PCR software. The primers and probe for the 18S (Hs03003631_g1) were purchased from Thermo Fisher Scientific. Va24 primers: Forward 5′-TGTCAAGCTGGTCGAGAAAAG-3′ Reverse: 5′-TCATGAGCAGATTAAACCCGG-3′ Probe 5′-CCACTTTCAGGAGGAGGATTCGGAAC-3′. Tyr-TRAC primers: Forward 5′-ACTTCGACAGCCAGATCAAC-3′ Reverse: 5′-TGTGAAGCTGGTCTGATTG -3′ Probe 5′-TGCTGGACATGAAGGCGATGGA-3′. Tyr-TRBC primers: Forward 5′-TGGGTCAACGGCAAAGAG-3′ Reverse: 5′-TGGCATCTGAAGTGGTTCC -3′ Probe 5′-CCGATCCCCAGGCCTACAAAGAG-3′.

Western blot

Three million tumor cells (M14-wt, M14-A2, C8161, or SK-MEL-5) were lysed with 81 μL of 2X Laemmil Sample Buffer (Bio Rad) and 9 μL of 2-mercaptoethanol (Fisher Scientific). Ten microliters of total protein lysates were separated by Mini-PROTEAN TGX Stain-Free Gels (Bio-Rad) electrophoresis. After protein transfer, membranes were incubated with 3 μL of anti-tyrosinase (Thermo Fisher, clone T311) or 15 μL of anti-MART-1 (Invitrogen, clone M2-7C10). After washes, membranes were incubated with 3 μL of HRP-conjugated goat anti-mouse IgG (H+L) secondary Ab (Invitrogen). Staining for β-actin (Santa Cruz Biotechnology) was used as loading control. Membranes were developed with SuperSignal West Femto Maximum Sensitivity Substrate (Thermo Scientific).

Cocultures and ELISAs

NKTs and $CD8^+$ T cells (10^5 cells/well) were cocultured with tumor cell lines (M14-wt, M14-A2, C8161, or SK-MEL-5; 10^5 cells/well) at an effector-to-target (E:T) ratio of 1:1 in 24-well plates, in complete medium, in the absence of cytokines. After 3 days of culture, cells were harvested and stained for CD3 (APC-H7, clone SK7 from BD Biosciences) and CD276 (BV421, clone 7-517 from BD Biosciences) monoclonal Abs (mAb) to detect T cells and tumor cells, respectively. Percentage of residual tumor cells in culture were enumerated by flow cytometry. NKTs (10^5 cells/well) were also cocultured with HLA-$A2^+$ T-cell blasts loaded with the YMDGTMSQV peptide (100 nmol/L) at an E:T ratio of 1:1 or activated with 10 μL of anti-Vα24 (clone 6B11, from BD Biosciences) in 1 mL of complete medium in the absence of cytokines. Culture supernatants were harvested after 24 hours of culture and IFNγ measured in 100 μL of supernatant with the DuoSet Human IFNγ ELISA kit (R&D Systems). Data acquisition was performed on a Synegrgy2 microplate reader (BioTek) using the Gen5 software.

ELISpot assay

The IFNγ ELISpot assay was performed as previously described (17). Briefly, 2×10^4 NKTs or $CD8^+$ T cells per well were plated in triplicate and then stimulated with 2×10^4 T2 cells loaded with specific peptides (YMDGTMSQV for the Tyr-TCR, ELAGIGILTV for the MART-1-TCR, or ALYVDSLFFL for the PRAME-TCR). NKTs and $CD8^+$ T cells were stimulated with PMA (25 ng/mL), ionomycin (1 μg/mL; both from Sigma-Aldrich), and IL2 (100 IU/mL) as a positive control. After 18 hours, IFNγ single-forming cells (SFC) were counted using the ELISpot reader (AID Classic ELR07) and analyzed using the Elispot7.0 software.

Study approval

All mouse experiments were performed in accordance with UNC Animal Husbandry and Institutional Animal Care and Use Committee (IACUC) guidelines and were approved by UNC IACUC (IACUC ID: 49268).

Xenograft models

Female and male NSG mice (7–9 weeks of age, obtained from the UNC Animal Core) were injected either subcutaneously (s.c.) with 0.5×10^6 SK-MEL-5 tumor cells or intravenously (i.v.) via tail injection with $0.5–1 \times 10^6$ FFluc-labeled M14-wt or M14-A2 tumor cells. In specific experiments, mice received low-dose irradiation (100 cGy) 24 hours before receiving i.v. 1×10^6 FFluc-labeled M14-A2 cells. Seven days after tumor cell injection (day 0) and at days +5 and +12, mice were infused i.v. with 1×10^7 or 5×10^6 nontransduced (NT)-NKTs or Tyr-TCR NKTs (expressing or not eGFP-FFluc, and nonsorted for TCR expression). In selected experiments, nontransduced (NT)-T cells and T cells expressing the Tyr-TCR (Tyr-TCR-Ts and nonsorted for TCR expression) were also used. In selected experiments, recombinant human IL2 (1000 U/mouse) was administered intraperitoneally (i.p.) every 2 days for a total of 8 doses after the

adoptive transfer of either NKTs or T cells. Melanoma tumor cell growth was monitored weekly either with caliper measurement for s.c. tumors, or by bioluminescence (BLI; total flux, photons/second) using the IVIS kinetic *in vivo* imaging system (PerkinElmer) for the metastatic models. Mice were sacrificed according to UNC guidelines for either tumor growth or occurrence of sign of discomfort, including graft-versus-mouse disease (weight loss, fur loss, and lethargy). When mice were sacrificed, peripheral blood was collected from the heart and spleen, liver, and tumor were smashed on cell strainers and washed with 2 mL of PBS. Peripheral blood, spleen, liver, and tumors were analyzed to detect the presence of NKTs or T cells [stained with Abs against CD3 (APC-H7, clone SK7) and CD45 (APC, clone 2D1)] by flow cytometry using CountBright absolute counting beads (Invitrogen). In selected experiments, tumors were isolated, homogenized in a total of 1 mL of PBS, and 100 μL of the supernatant were used to measure the human IFNγ using the DuoSet Human IFNγ ELISA kit (R&D Systems). Infiltrating NKTs were counted in the tumors by staining with Abs against CD3 (APC-H7, clone SK7) and CD45 (APC, clone 2D1) and counting beads (Invitrogen) and analyzing via flow cytometry.

Statistical analysis

Data were summarized as the mean ± SD. Student *t* test or two-way ANOVA were used to determine statistically significant differences between treatment groups, with Bonferroni's correction for multiple comparisons when appropriate (Prism 6: GraphPad Software). Survival analysis was performed using the Kaplan–Meier method (Prism 6: GraphPad Software). All *P* values less than 0.05 were considered statistically significant.

Results

NKTs can be engineered to express an ectopic TCR

Isolated and cultured NKTs (**Fig. 1A**) robustly and consistently expanded *ex vivo* (fold increase: 17 ± 4 after the first stimulation, S1; **Fig. 1B**). By days 5 to 7 of culture (before retroviral transduction), 93% ± 4% of the isolated cells expressed the iTCR, as assessed by flow cytometry using a specific tetramer (**Fig. 1B**). As a proof of concept, NKTs were transduced with a gamma retroviral vector to express an HLA-A2–restricted, tyrosinase-specific TCR (Tyr-TCR; ref. 19). Tyr-TCR was detectable in 76% ± 8% NKTs (Tyr-TCR NKTs), and the expression remained stable over the course of the entire culture period (**Fig. 1C**). The growth kinetics of NKTs was not hampered by the expression of the Tyr-TCR, as $1.2 \times 10^8 \pm 8.5 \times 10^7$ cells were obtained at the end of the culture period (S2), a number that is sufficient for clinical adoptive transfer (**Fig. 1D**). Tyr-TCR NKTs retained the phenotypic characteristics of nontransduced NKTs, including preservation of CD4 and CD8 composition and expression of CD62L and exhaustion markers (**Fig. 1E**). Tyr-TCR NKTs showed HLA class I restriction, as they lysed HLA-$A2^+$ PHA blasts loaded with the HLA-A*0201 tyrosinase YMD peptide (77% ± 28% lysis at the E:T ratio of 40:1), whereas control NKTs (NT-NKTs) showed negligible cytotoxic activity (**Fig. 1F**). Overall, NKTs could be successfully manipulated to express a functional MHC class I–restricted TCR.

An ectopic TCR displaces the iTCR for expression on the cell surface in NKTs

As early as 3 to 4 days after retroviral transduction with the Tyr-TCR–expressing vector, Tyr-TCR NKTs consisted of two distinct subsets, namely, $CD3^+iTCR^+$ (59% ± 18%) and $CD3^+iTCR^-$ (41% ± 18%) cells (**Fig. 2A**). A similar downregulation of the iTCR was observed when NKTs were transduced with gamma retroviral vectors encoding other HLA-A2–restricted TCRs specific for survivin (Sur-TCR), PRAME (PRAME-TCR), and MART-1 (MART-1-TCR) antigens (Supplementary Fig. S1A), thus excluding that the observed emergence of $CD3^+iTCR^-$ NKTs was an exclusive phenomenon caused by the Tyr-TCR. Staining with iTCR and Tyr-TCR multimers revealed three distinct cell subsets: $iTCR^-Tyr\text{-}TCR^+$ (44% ± 15%), $iTCR^+Tyr\text{-}TCR^+$ (34% ± 11%), and $iTCR^+Tyr\text{-}TCR^-$ (19% ± 11%) cells. These three subsets were also identified when using other combinations of Abs (Vα24, Vβ11, and Vβ12 Abs) recognizing Tyr-TCR and iTCR (**Fig. 2B**). Using SupT1 cells ($CD3^+TCR^-$; ref. 26), we observed that ectopic TCRs outcompeted iTCRs for cell-surface expression (Supplementary Fig. S1B) and that iTCRs were retained within the cytoplasm (Supplementary Fig. S1C). When $iTCR^+Tyr\text{-}TCR^+$ and $iTCR^-Tyr\text{-}TCR^+$ NKTs were sorted, the Vα24 chain of the iTCR was detectable in both subsets by confocal microscopy but was confined to the cytoplasm in $iTCR^-Tyr\text{-}TCR^+$ NKTs, whereas it was expressed on the cell surface in $iTCR^+Tyr\text{-}TCR^+$ NKTs (**Fig. 2C**). Based on these results, we hypothesized that in $iTCR^-Tyr\text{-}TCR^+$ NKTs, the Tyr-TCR displaced the iTCR for CD3 usage, and as a consequence, it was preferentially transferred to the cell surface. To corroborate this premise, we transduced NKTs with a retroviral vector encoding the CD3γδεζ genes (6) to provide an excess of CD3 to NKTs, and confirmed an increase of CD3 molecules on the cell surface (**Fig. 2D**). When $Tyr\text{-}TCR^-$ NKTs were transduced with the CD3 encoding vector, we observed an increase of the $iTCR^+Tyr\text{-}TCR^+$ subset (from 34% ± 14% to 72% ± 3%, gated on $Tyr\text{-}TCR^+$ cells, $P < 0.0001$; **Fig. 2E**). Overall, these data indicated that the ectopic TCR can displace the iTCR from CD3 binding in NKTs.

Higher transcripts of the ectopic TCR outcompete the endogenous iTCR

We then studied how the transgenic TCR displaces the endogenous iTCR in NKTs. We first analyzed if $iTCR^+Tyr\text{-}TCR^+$ and $iTCR^-Tyr\text{-}TCR^+$ subsets showed differences in coreceptor expression, but both CD4 and CD8 were equally distributed within the two subsets (**Fig. 3A**). Although the Vα24-Jα18 chain is known to preferentially pair with Vβ11 (TRBV25-1) chains in human NKTs (16), we explored if combination with distinct Vβ chains correlated with the specific NKTs subsets. $iTCR^+Tyr\text{-}TCR^+$ and $iTCR^-Tyr\text{-}TCR^+$ were sorted using specific TCR multimers (Supplementary Fig. S2A) and subsequently analyzed for TCRβ using RNA amplicon sequencing. Although TRBV25-1 was the dominant detected TCR Vβ chain (range, 90.54%–96.49%), a proportion of the repertoire was distributed across the other 47 Vβ chains (**Fig. 3B**). However, TCR Vβ chain distribution was conserved between $iTCR^+Tyr\text{-}TCR^+$ and $iTCR^-Tyr\text{-}TCR^+$ subsets, suggesting that the TCR Vβ repertoire differences did not segregate for iTCR expression. The majority of shared TCR clones (identified by the CDR3 sequence of the Vβ chain) was observed within each donor rather than within the $iTCR^+Tyr\text{-}TCR^+$ or $iTCR^-Tyr\text{-}TCR^+$ subsets (Supplementary Fig. S2B), indicating that the type of TCR Vβ chain associated with the Vα24-Jα18 was not affecting the binding with CD3, and thus the iTCR displacement in $iTCR^-Tyr\text{-}TCR^+$ NKTs.

We next reasoned that the iTCR expression may be associated with transgene integrant copy-number variations between the $iTCR^+Tyr\text{-}TCR^+$ and $iTCR^-Tyr\text{-}TCR^+$ subsets. We assessed the mRNA expression of both Tyr-TRAC and Tyr-TRBC chains (transgenic TCR) and of Vα24 (iTCR) in both $iTCR^+Tyr\text{-}TCR^+$ and $iTCR^-Tyr\text{-}TCR^+$ subsets and found the mRNA of both Tyr-TCR chains to be significantly higher than the mRNA expression of the iTCR chain (**Fig. 3C**). Both

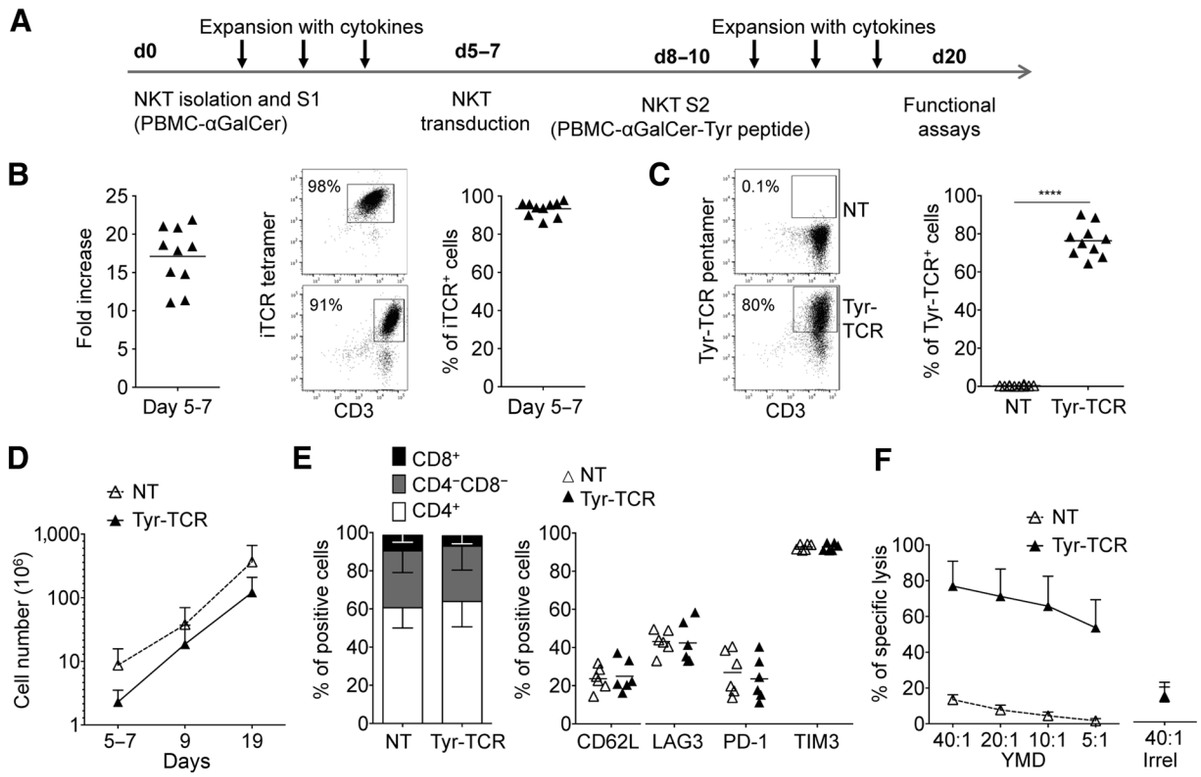

Figure 1.

NKTs can be genetically modified to express an HLA-A2–restricted tyrosinase-specific TCR (Tyr-TCR). **A,** Schematic timeline of the protocol used to select, transduce, and expand NKTs. S1 and S2 indicate the first and second stimulation, respectively. **B,** Fold increase (left), representative flow cytometry plots (middle), and purity of NKTs (right) on days 5 to 7 after S1 ($n = 10$, mean shown). **C,** Representative flow cytometry plots (left) and summary (right) of Tyr-TCR expression by control (NT-NKTs) and transduced (Tyr-TCR NKTs) NKTs assessed at day 19 of culture ($n = 10$, mean shown). ****, $P < 0.0001$, paired t test. **D,** Total cell numbers of NT-NKTs and Tyr-TCR NKTs at day 19 ($n = 10$, mean + SD shown). **E,** Phenotypic characterization of NT-NKTs and Tyr-TCR NKTs at days 19 to 20 of culture ($n = 6$, mean shown). **F,** NT-NKTs and Tyr-TCR NKTs were tested in a 5-hour ^{51}Cr-release assay against different ratios of HLA-A2$^+$ PHA blasts loaded with either the specific tyrosinase peptide (YMD) or an irrelevant MART-1 peptide (Irrel, ELAGIGLTV) at the concentration of 100 nmol/L ($n = 4$, mean + SD shown).

Tyr-TCR chains were more significantly expressed in iTCR$^-$Tyr-TCR$^+$ cells than in the iTCR$^+$Tyr-TCR$^+$ subset ($P = 0.0004$; **Fig. 3C**). The higher mRNA expression of Tyr-TRAC and Tyr-TRBC chains in iTCR$^-$Tyr-TCR$^+$ NKTs reflected the higher copy numbers of the transgene integrants (**Fig. 3D**). We then analyzed the functionality of sorted iTCR$^+$Tyr-TCR$^+$ and iTCR$^-$Tyr-TCR$^+$ NKTs and found that it was independent from the expression of the iTCR because only the iTCR$^+$Tyr-TCR$^+$ subset released IFNγ in response to the agonistic Vα24 mAb (clone 6B11; **Fig. 3E**), but both iTCR$^+$Tyr-TCR$^+$ and iTCR$^-$Tyr-TCR$^+$ subsets lysed and produced IFNγ in response to HLA-A2$^+$ PHA blasts loaded with the HLA-A*0201–restricted YMD peptide (**Fig. 3F**). Overall, these data suggest that the ectopic TCR outcompeted the iTCR for CD3 binding when the α- and β-TCR chains were expressed at higher levels than iTCR chains, so that the HLA-restricted cytotoxic activity of TCR NKTs could be exploited regardless of the presence of the iTCR on the cell surface.

Tyr-TCR NKTs acquire HLA-A2–restricted cytotoxic activity against tumor cells

To measure the antitumor activity of Tyr-TCR NKTs against tumor cells expressing tyrosinase, we used the HLA-A2$^+$Tyr$^+$ melanoma cell line SK-MEL-5. The HLA-A2$^+$Tyr$^-$ melanoma cell line C8161 was used as a negative control. As additional controls, we tested the melanoma cell line M14 that is HLA-A2$^-$Tyr$^+$ (M14-wt) and the same cell line genetically modified to express the HLA-A2 molecule (M14-A2; **Fig. 4A**). Tyr-TCR NKTs consistently lysed the HLA-A2$^+$Tyr$^+$ M14-A2 and SK-MEL-5 cells but not the HLA-A2$^-$Tyr$^+$ (M14-wt) or HLA-A2$^+$Tyr$^-$ (C8161) tumor cells (**Fig. 4B**). Both iTCR$^+$Tyr-TCR$^+$ and iTCR$^-$Tyr-TCR$^+$ NKT subsets lysed the M14-A2 and SK-MEL-5 cells (Supplementary Fig. S3A). We then cocultured Tyr-TCR NKTs and control NT-NKTs with these melanoma cell lines for 3 days. Both M14-A2 and SK-MEL-5 cells were efficiently eliminated (<3% residual tumor cells) by Tyr-TCR NKTs, whereas M14-wt and C8161 cells overgrew and accounted for more than 85% of the cells at the end of the 3-day culture (**Fig. 4C**). NT-NKTs did not eliminate any of these tumor cells. The antitumor activity of Tyr-TCR NKTs was paralleled by IFNγ production, which was detected only when Tyr-TCR NKTs were cocultured with M14-A2 and SK-MEL-5 cells (**Fig. 4D**). The IFNγ production in response to melanoma cell lines was comparable in both iTCR$^+$Tyr-TCR$^+$ and iTCR$^-$Tyr-TCR$^+$ NKT subsets (Supplementary Fig. S3B). Overall, these data demonstrated the antitumor activity of NKTs genetically modified to express an HLA-A2–restricted TCR.

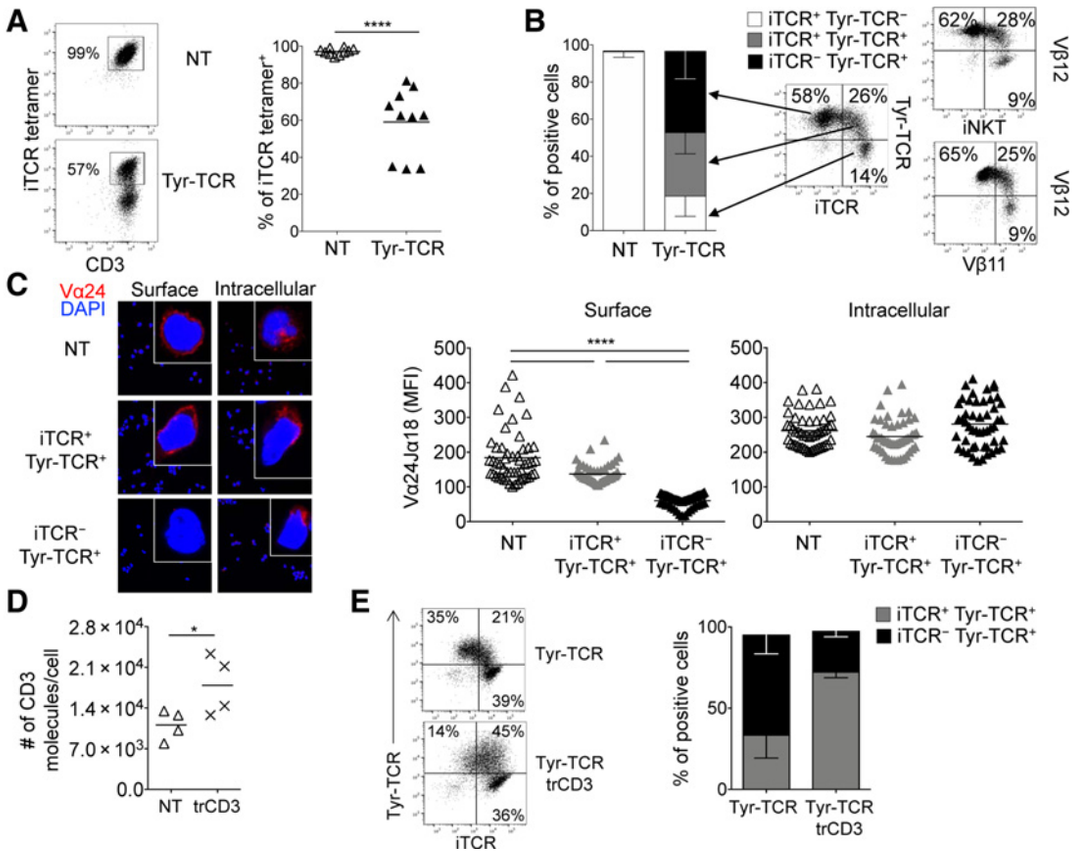

Figure 2.

Transgenic TCRs outcompete the iTCR for expression on the cell surface in NKTs. **A,** Representative flow cytometry plots (left) and summary (right) illustrating the expression of the iTCR in NT-NKTs and Tyr-TCR NKTs 4 days after transduction ($n = 10$, mean shown). ****, $P < 0.0001$, paired t test. **B,** Subset composition of NT-NKTs and Tyr-TCR NKTs at the end of S2 (days 18–20) defined by expression of iTCR and Tyr-TCR detected by specific pentamers ($n = 10$, left, SD shown). Representative flow cytometry plots illustrating the expression of the iTCR (stained alternatively with the iTCR tetramer, anti-Vα24, or anti-Vβ11), and the Tyr-TCR (stained with either the Tyr-TCR pentamer or anti-Vβ12; right). **C,** Surface and intracellular staining of sorted iTCR$^+$Tyr-TCR$^-$, iTCR$^-$Tyr-TCR$^+$, and iTCR$^+$Tyr-TCR$^+$ NKT subsets with the Vα24Jα18 Ab (red staining). The blue staining indicates the DAPI. Shown are representative images of a single field of view taken via confocal microscopy (magnification, 63×). Graphs show the summary of the mean fluorescence intensities (MFI) for surface and intracellular staining ($n = 50$, right, mean shown). MFI was calculated on NKTs obtained from 4 images for each condition. ****, $P < 0.0001$, unpaired t test. **D,** Number of CD3 molecules per cell in control NKTs (NT) and NKTs transduced with a vector encoding the CD3 complex (trCD3; $n = 4$, mean shown). *, $P = 0.0151$, paired t test. **E,** Representative flow cytometry plots (left) and summary (right) illustrating the percentage of iTCR$^-$Tyr-TCR$^+$ and iTCR$^+$Tyr-TCR$^+$ cells gated on Tyr-TCR$^+$ NKTs, in NKTs transduced with the Tyr-TCR encoding vector alone (Tyr-TCR NKTs) and in NKTs cotransduced with the vectors encoding the Tyr-TCR and CD3 (Tyr-TCR-trCD3 NKTs; $n = 5$, SD shown).

High-functional avid TCRs are required to generate TCR-redirected NKTs

To assess if TCR avidity played a role in determining the anti-tumor activity of TCR-redirected NKTs, we used NKTs expressing an HLA-A2–restricted MART-1–specific TCR (MART-1-TCR), which is characterized by lower functional avidity compared with the Tyr-TCR (19). Transduction of NKTs with MART-1–TCR was comparable with that of Tyr-TCR (75% ± 13% vs. 78% ± 10%, respectively; **Fig. 5A**) and also in terms of expression [MART-1–TCR mean fluorescence intensity (MFI) = 22,377 ± 1,753 vs. Tyr-TCR MFI = 19,461 ± 2,336; Supplementary Fig. S4A]. However, MART-1–TCR NKTs had less IFNγ spot-forming cells against T2 cells loaded with decreasing concentrations of the specific peptide compared with Tyr-TCR NKTs (**Fig. 5B**), despite TCRs being expressed at comparable levels. Similarly, MART-1–TCR NKTs showed lower cytotoxic activity against HLA-A2$^+$ PHA blasts loaded with the specific peptide than Tyr-TCR NKTs (**Fig. 5C**). In contrast, when expressed in CD8$^+$ T cells, both Tyr-TCR and MART-1–TCR (**Fig. 5D**) showed similar functionality to one another, assessed by IFNγ SFCs in response to peptide-loaded T2 cells (**Fig. 5E**) and cytotoxic activity against peptide-loaded HLA-A2$^+$ PHA blasts (**Fig. 5F**). We also compared the antitumor activity of Tyr-TCR– and MART-1-TCR–expressing T cells and NKTs against the SK-MEL5 cell line, which expresses both tyrosinase and MART-1 (**Fig. 5G**). Although CD8$^+$ T cells expressing either the Tyr-TCR or MART-1–TCR eliminated HLA-A2$^+$Tyr$^+$MART-1$^+$ melanoma cells in coculture experiments (**Fig. 5H**), only Tyr-TCR NKTs successfully eliminated these tumor cells (**Fig. 5I**). These data were confirmed using another low-affinity HLA-A2-restricted TCR specific for PRAME (PRAME-TCR). As observed for the MART-1-TCR, despite comparable transduction efficiency and MFI (Supplementary Fig. S4B), PRAME-TCR-NKT

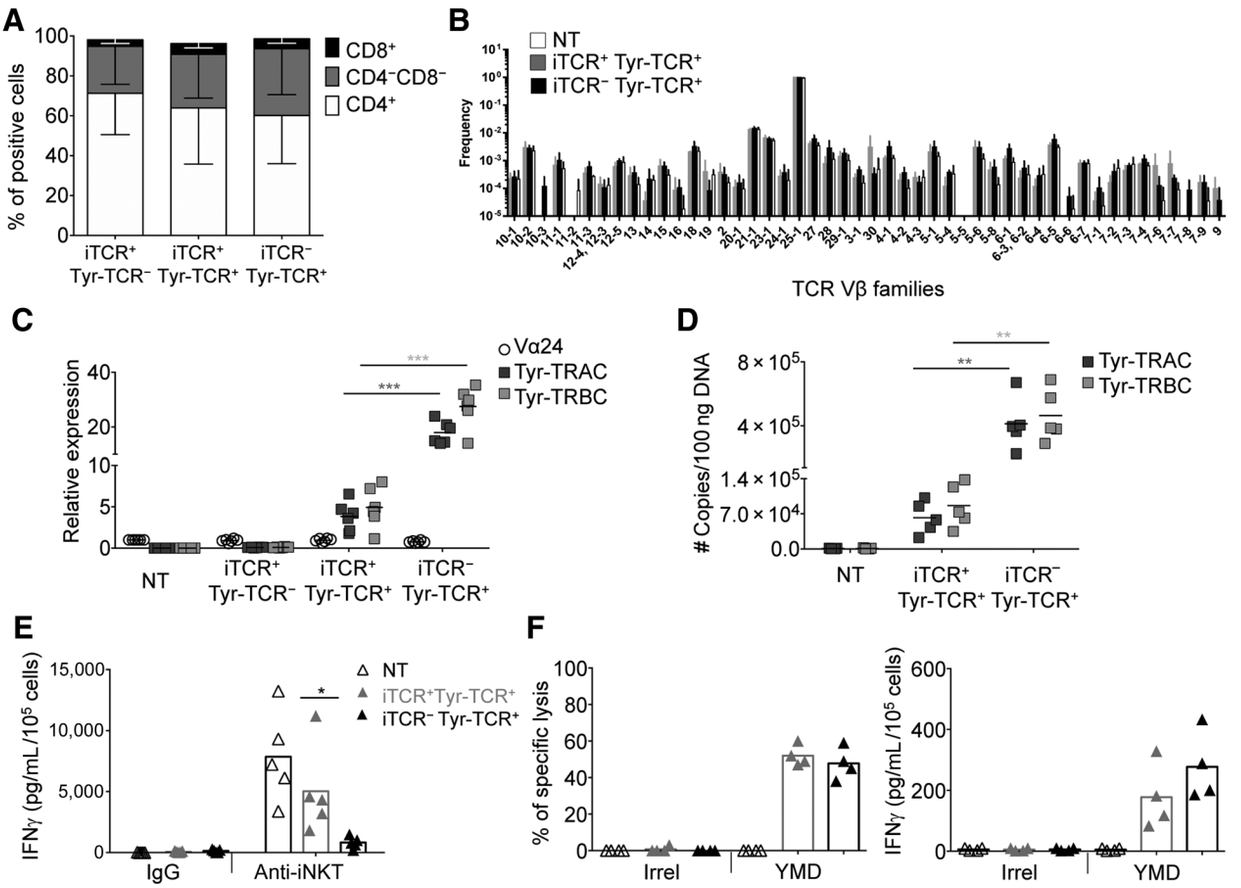

Figure 3.

Tyr-TCR function in NKTs does not require the presence of the iTCR. **A,** CD4/CD8 composition in each subset of Tyr-TCR NKTs ($n = 3$, SD shown). **B,** Frequency of TCR Vβ chain RNA in NT-NKTs, iTCR$^+$Tyr-TCR$^+$ NKTs, and iTCR$^-$Tyr-TCR$^+$ NKTs obtained after sorting and TCR amplicon RNA sequencing of each subset (SD shown). **C,** Relative expression of the TCR Vα24 chain for the iTCR, and of TCRα (Tyr-TRAC) and TCRβ (Tyr-TRBC) chains for Tyr-TCR assessed by qPCR in NT-NKTs, iTCR$^+$Tyr-TCR$^-$, iTCR$^+$Tyr-TCR$^+$, and iTCR$^-$Tyr-TCR$^+$ NKT subsets ($n = 6$, mean shown). ***, $P = 0.0004$ for Tyr-TRAC; ***, $P = 0.0002$ for Tyr-TRBC, paired t test. **D,** Quantitation of TCRα (Tyr-TRAC) and TCRβ (Tyr-TRBC) copy number of integrated transgene via qPCR in NT-NKTs, iTCR$^+$Tyr-TCR$^+$, and iTCR$^-$Tyr-TCR$^+$ NKT subsets ($n = 5$, mean shown). **, $P = 0.0087$ for Tyr-TRAC; **, $P = 0.0062$ for Tyr-TRBC, paired t test. **E,** Quantification of IFNγ in supernatants collected after 24 hours from the activation of NT, iTCR$^-$Tyr-TCR$^+$, and iTCR$^+$Tyr-TCR$^+$ NKTs with the Vα24 Ab. Isotype control was used as negative control ($n = 5$, mean shown). *, $P = 0.0139$, paired t test. **F,** iTCR$^-$Tyr-TCR$^+$ and iTCR$^+$Tyr-TCR$^+$ NKTs were tested in a 5-hour ^{51}Cr-release assay (E:T = 40:1) against HLA-A2$^+$ PHA blasts loaded with an irrelevant MART-1 peptide (Irrel, ELAGIGLTV) or with the YMD peptide (100 nmol/L; left; $n = 4$, mean shown). Quantification of IFNγ in supernatants collected after 24 hours from the cocultures (E:T = 1:1) of iTCR$^-$Tyr-TCR$^+$ or iTCR$^+$Tyr-TCR$^+$ NKTs with HLA-A2$^+$ PHA blasts loaded with an irrelevant peptide (Irrel) or with the YMN peptide (100 nmol/L; right; $n = 4$, mean shown).

functions were inferior to those of PRAME-TCR-Ts, as the former had less IFNγ SFCs against T2 cells loaded with decreasing concentrations of the specific peptide (Supplementary Fig. S4C) and showed an inferior cytotoxic activity against peptide-loaded HLA-A2$^+$ PHA blasts (Supplementary Fig. S4D).

Because CD8$^+$ T cells expressing either MART-1-TCR or Tyr-TCR were equally effective, we explored if the functionality of MART-1-TCR NKTs, that were mostly CD4$^+$ or CD4$^-$CD8$^-$ cells, could be rescued by overexpressing the CD8α subunit, as previously reported for CD4$^+$ T cells (27). Coexpression of both a MART-1-TCR and human CD8α (>60% CD8α$^+$), this modification failed to enhance the functional avidity of MART-1-TCR NKTs (Supplementary Fig. S5A–S5C). Thus, our data suggest that the intrinsic functional avidity of the TCR was critical to functionally redirect NKT activity via HLA class I–restricted TCRs.

Tyr-TCR NKTs provide antitumor effects *in vivo*

Having shown that functional avid Tyr-TCR grants the antigen specificity of NKTs *in vitro*, we used a xenogeneic NSG melanoma mouse model to assess if Tyr-TCR NKTs controlled tumor growth *in vivo*. NKTs were administered i.v. in mice engrafted s.c. with the melanoma cell line SK-MEL-5 (**Fig. 6A**). Tyr-TCR NKTs exhibited superior control of tumor growth than NT-NKTs (317 mm^3 ± 124 mm^3 vs. 1121 mm^3 ± 216 mm^3, respectively, at day 64, $P < 0.0001$; **Fig. 6B**; Supplementary Fig. S6A). None of the NKT-treated mice developed signs of graft-versus-mouse toxicity. In harvested tumors, we observed a higher number of infiltrating NKTs in mice treated with Tyr-TCR NKTs compared with NT-NKTs (997 ± 650 NKTs vs. 351 ± 401 NKTs, respectively) and higher detection of IFNγ release (183.5 pg/mL ± 179.1 pg/mL vs. 12.1 pg/mL ± 13.7 pg/mL, respectively; **Fig. 6C**), suggesting that

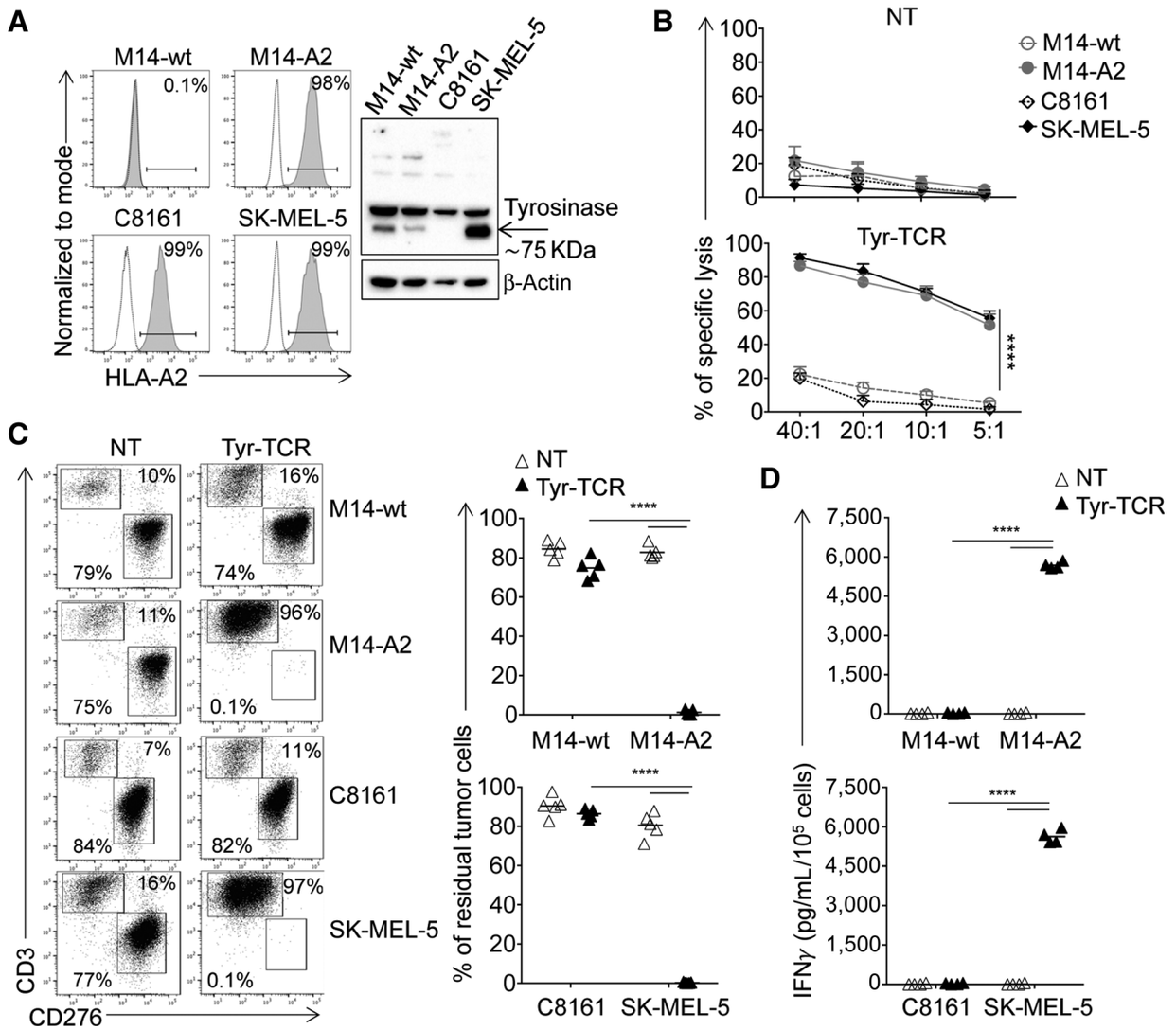

Figure 4.

Tyr-TCR NKTs target HLA-A2$^+$Tyr$^+$ cells. **A,** Expression of the HLA-A2 molecule in melanoma cell lines assessed by flow cytometry (left). Dotted and solid lines represent the isotype and HLA-A2 mAbs, respectively. The M14-wt cell line was modified to express the HLA-A2 molecule (M14-A2) via retroviral gene transfer. Detection of tyrosinase in lysates of the indicated melanoma cell lines assessed by Western blot (right). Staining for β-actin was used as a loading control. **B,** NT-NKTs (top graph) and Tyr-TCR NKTs (bottom graph) were tested against the melanoma cell lines in a 5-hour ^{51}Cr-release assay ($n = 4$, mean + SD shown). ****, $P < 0.0001$, two-way ANOVA with Bonferroni correction. **C,** NT-NKTs and Tyr-TCR NKTs were cocultured with melanoma cell lines (E:T = 1:1) for 3 days. Cells were then collected and stained with the CD3 and CD276 mAbs to identify NKTs and melanoma cells, respectively, by flow cytometry. Representative flow plots (left) and summary of the quantification of residual tumor cells in the culture (right, $n = 5$, mean shown). ****, $P < 0.0001$, paired t test. **D,** Quantification of IFNγ production in the supernatant collected after 24 hours of coculture of NT-NKTs and Tyr-TCR NKTs (E:T = 1:1; $n = 4$, mean shown). ****, $P < 0.0001$, paired t test.

Tyr-NKTs were functional at the tumor site. In contrast, no difference in the numbers of Tyr-TCR NKTs and NT-NKTs was detected in peripheral blood, liver, and spleen, and the expression of the Tyr-TCR was detectable in all the Tyr-TCR NKTs isolated (Supplementary Fig. S6B and S6C).

To further assess *in vivo* the HLA restriction of the antitumor responses mediated by Tyr-TCR NKTs, we also generated a metastatic murine model in which NSG mice were injected i.v. with either M14-wt or M14-A2 cells modified to express the enhanced green fluorescent protein (eGFP) and the firefly luciferase gene (FFLuc or eGFP-FFLuc). Tumor bioluminescence (BLI) was reduced only in mice engrafted with M14-A2 cells and treated with Tyr-TCR NKTs ($P < 0.0001$; **Fig. 6D**). When euthanized between days 41 and 63, the number of liver tumor metastases in M14-A2 tumor–bearing mice was significantly reduced compared with M14-wt tumor–bearing mice (1 ± 2 vs. 30 ± 13, $P < 0.0001$; **Fig. 6E**). In the same mouse model, we also assessed *in vivo* the persistence of Tyr-TCR NKTs using NKTs labeled with eGFP-FFLuc and unlabeled tumor cells. Tyr-TCR NKT BLI was detectable for 7 days after infusion (**Fig. 6F**). NKT persistence was also corroborated by phenotypic analyses in the peripheral blood and spleen ($1.6\% \pm 0.2\%$ and $0.9 \pm 1.2\%$ hCD3$^+$hCD45$^+$ cells, respectively) of treated mice (**Fig. 6G**). To assess if Tyr-TCR NKTs produced

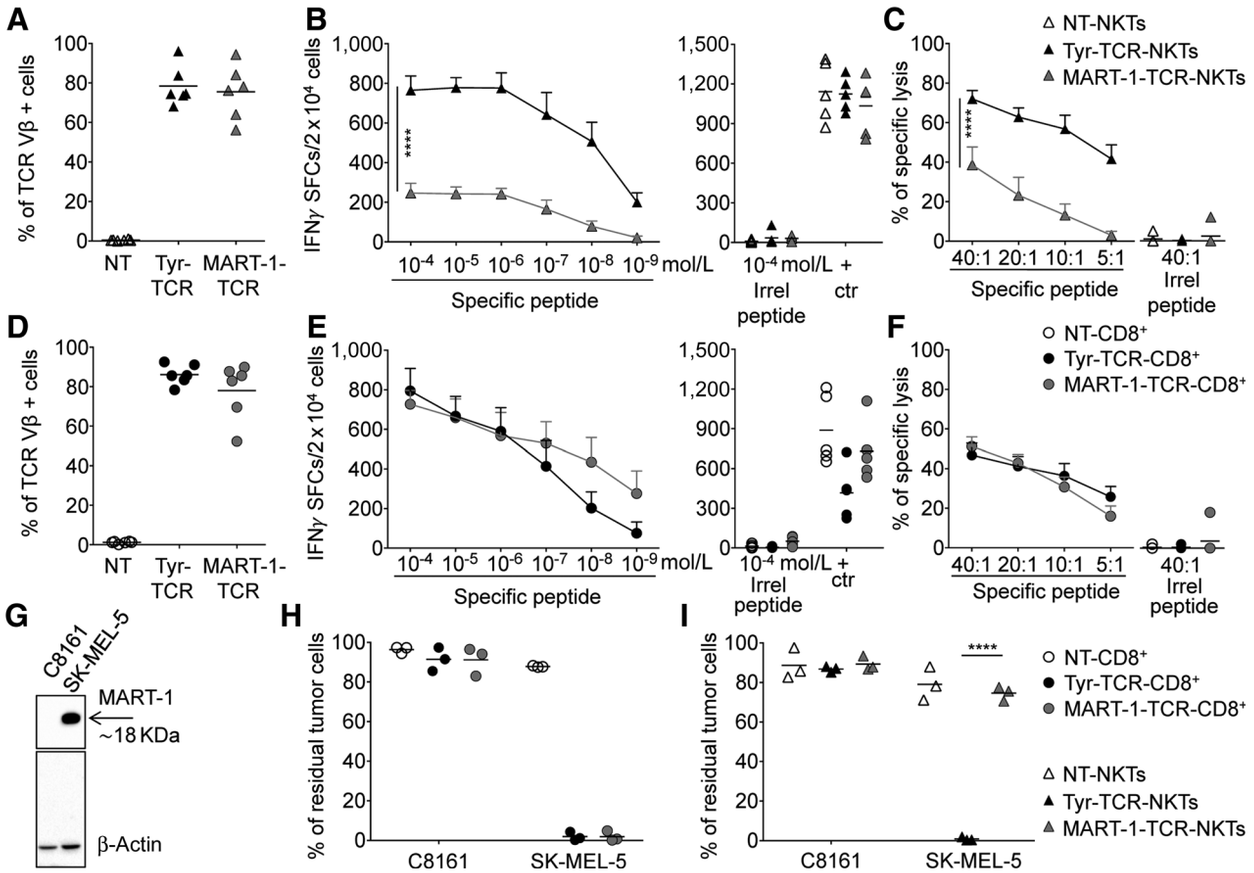

Figure 5.

A high-affinity TCR is required to redirect NKT specificity. Expression of Tyr-TCR and MART-1-TCR in NKTs (**A**) and CD8$^+$ T cells (**D**), assessed with an Ab specific for the TCR Vβ12 chain, 3 days after transduction ($n = 6$, mean shown). NT-NKTs and NT-CD8$^+$ T cells were also used as controls. TCR functional avidity assessed by IFNγ ELISpot assays for Tyr-TCR and MART-1-TCR in NKTs (**B**) and CD8$^+$ T cells (**E**) against T2 cells loaded with decreasing concentrations of the specific peptide (left graphs). T2 cells loaded with an irrelevant peptide or PMA/ionomycin/IL2 (+ctr) were used as negative and positive controls, respectively (right graphs, $n = 5$, mean + SEM shown). ****, $P < 0.0001$, two-way ANOVA with Bonferroni correction. SFCs, spot-forming cells. Cytotoxic activity assessed in a 5-hour ^{51}Cr release assay for NT, Tyr-TCR, and MART-1-TCR NKTs (**C**) and CD8$^+$ T cells (**F**) against HLA-A2$^+$ PHA blasts pulsed with either the specific peptide or an irrelevant peptide (Irrel, ELAGIGLTV) at the concentration of 100 nmol/L ($n = 5$, mean + SD shown). ****, $P < 0.0001$ by two-way ANOVA with Bonferroni correction. **G,** Detection of MART-1 in lysates of melanoma cell lines assessed by Western blot. Staining for β-actin was used as a loading control. NT, Tyr-TCR, and MART-1-TCR CD8$^+$ T cells (**H**) and NKTs (**I**) were cocultured with SK-MEL5 or C8161 (E:T = 1:1) for 3 days. Cells were then collected and stained with the CD3 and CD276 Abs to identify NKTs/CD8$^+$ T cells and tumor cells, respectively, by flow cytometry. Quantification of the residual tumor cells in the culture ($n = 3$, mean shown). ****, $P < 0.0001$, paired *t* test.

superior antitumor control when their persistence was prolonged, we infused multiple doses of Tyr-TCR NKTs and compared the efficacy of Tyr-TCR NKTs and Tyr-TCR-Ts generated from the same donors (**Fig. 7A**). Both Tyr-TCR NKTs and Tyr-TCR-Ts, which were detectable in the circulation up to days 40 to 60 (**Fig. 7B**), successfully controlled tumor growth (**Fig. 7C** and **D**) and produced an improved overall survival compared with NT-NKTs and NT-Ts ($P < 0.0001$; **Fig. 7E**). The number of liver tumor metastases was significantly reduced in mice treated with either the Tyr-TCR NKTs or the Tyr-TCR-Ts compared with NT-NKTs and NT-Ts ($P < 0.0001$; Supplementary Fig. S6D). Tyr-TCR NKTs and Tyr-TCR-Ts were detectable in both the liver and spleen of mice sacrificed between days 40 and 60 (Supplementary Fig. S6E). However, 11 of the 18 mice (61%) receiving Tyr-TCR-Ts developed lethal graft-versus-mouse disease characterized by weight and fur loss and lethargy (**Fig. 7F**). This graft-versus-mouse disease also confounded the observed long-term tumor control mediated from the Tyr-TCR-Ts. Finally, we used the same *in vivo* models, but decreased the number of T cells and NKTs injected (5×10^6 cells/injection; Supplementary Fig. S7A). The antitumor activity of Tyr-TCR NKTs and Tyr-TCR-Ts treated mice was comparable (Supplementary Fig. S7B–S7D), and the Tyr-TCR-Ts continued to cause a lethal graft-versus-mouse effect (Supplementary Fig. S7E). Thus, our data indicated that TCR NKTs could control tumor growth *in vivo* without causing reactivity against murine tissues.

Discussion

We showed that the antigen specificity of human NKTs could be redirected toward tumor antigens by inserting an ectopic TCR. Our study critically outlined the advantages of using this platform for the expression of ectopic TCRs, namely, how the TCR could outcompete

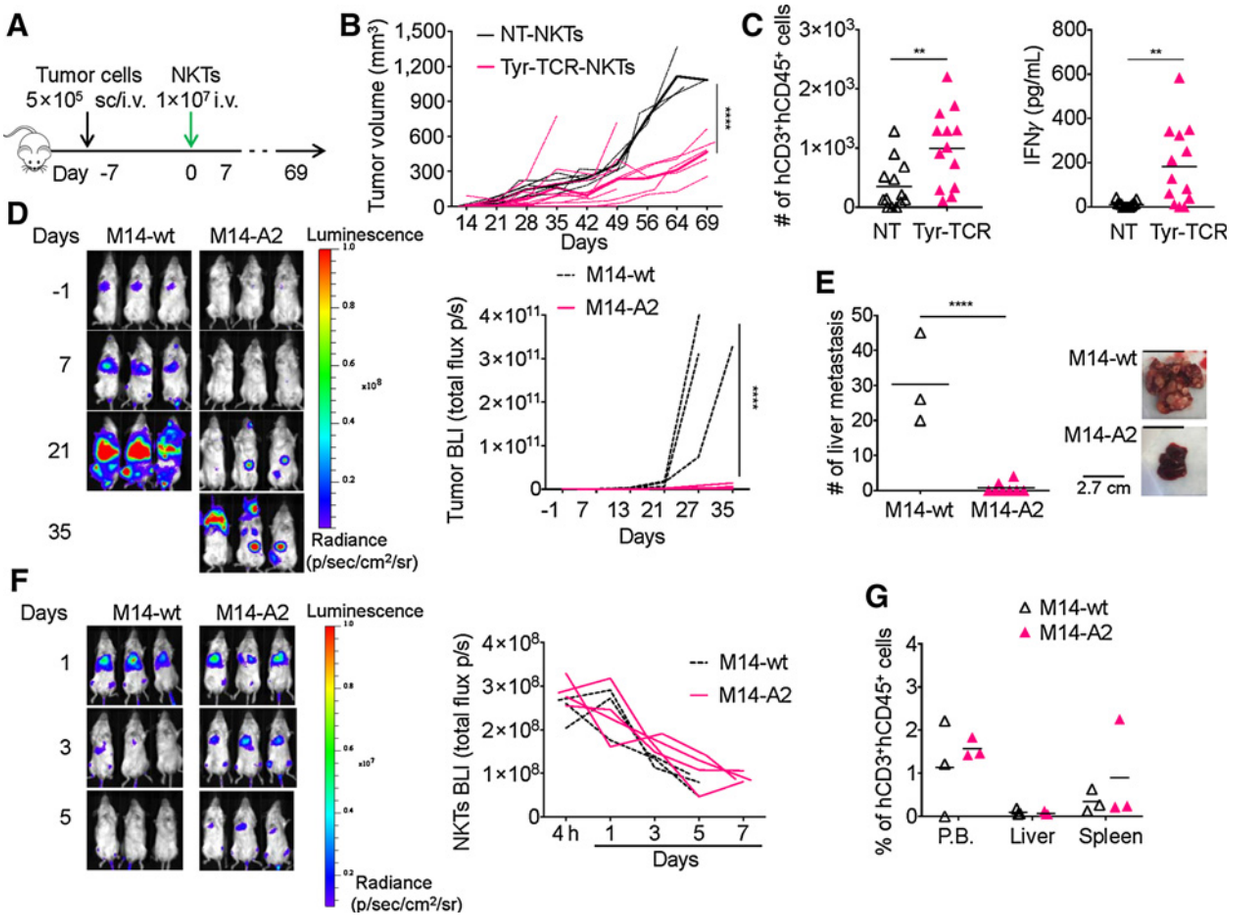

Figure 6.

Tyr-TCR NKTs control the growth of HLA-A2$^+$Tyr$^+$ cells *in vivo*. **A,** Schema of the xenograft tumor model in NSG mice engrafted s.c. with SK-MEL-5 cells or i.v. with M14 cells and treated 1 week later with NKTs. **B,** Tumor growth in mice engrafted s.c. with SK-MEL-5 tumor cells and treated with NT-NKTs ($n = 5$) or Tyr-TCR NKTs ($n = 10$). Dotted lines represent individual mice, and bolded solid lines represent the mean for the group. ****, $P < 0.0001$, two-way ANOVA with Bonferroni correction. **C,** Quantification of human CD3$^+$CD45$^+$ cells (left) and IFNγ (right) in each tumor harvested from mice engrafted with SK-MEL-5 tumor cells and treated with either NT-NKTs ($n = 13$) or Tyr-TCR NKTs ($n = 13$; mean shown). **, $P = 0.0055$; **, $P = 0.0021$, respectively, unpaired *t* test. **D,** Representative tumor BLI (left; color scale: min = 4.00×10^6; max = 1.00×10^8) and BLI kinetics of all treated mice (right) engrafted i.v. with eGFP-FFLuc–labeled M14-wt ($n = 3$) or M14-A2 ($n = 8$) tumor cells. ****, $P < 0.0001$, two-way ANOVA with Bonferroni correction. p/sec or p/s, photons/second. **E,** Mice engrafted with eGFP-FFLuc–labeled M14-wt ($n = 3$) or M14-A2 ($n = 8$) and treated with Tyr-TCR NKTs were euthanized, and tumor liver metastases counted (left, mean shown). Representative images of the livers (right). ****, $P < 0.0001$, unpaired *t* test. **F,** Mice were infused i.v. with 1×10^6 M14-wt or M14-A2 cells, and after 7 days, they were injected with 1×10^7 Tyr-TCR NKTs labeled with eGFP-FFluc. Representative Tyr-TCR NKTs BLI (left; color scale: min = 1.00×10^6; max = 1.00×10^7) and BLI kinetics of all mice (right) of M14-wt ($n = 3$) or M14-A2 ($n = 4$) tumor–bearing mice. p/sec or p/s, photons/second. **G,** Quantification of human CD3$^+$CD45$^+$ cells in the peripheral blood (P.B.), liver, and spleen of M14-wt ($n = 3$) or M14-A2 ($n = 3$) tumor–bearing mice treated with Tyr-TCR NKTs (mean shown).

the iTCR for the cell-surface expression without the need for additional manipulation to knockdown endogenous TCR chains as required in T cells.

Adoptive transfer of polyclonal T cells expressing high-affinity TCRs have shown promising clinical responses (28). However, current issues related to ectopic TCR expression in T cells suggest that exploring alternative platforms for TCR expression may be beneficial to further enhance clinical activity and safety of TCR-engineered cells. We previously demonstrated that NKTs can be engineered to express a chimeric antigen receptor for redirected tumor target capabilities (29). Jiang and colleagues previously showed that an HLA class I–restricted TCR targeting an epitope of the 38-kDa protein of the Mycobacterium tuberculosis can be expressed by NKTs and react against DCs pulsed with the 38-kDa protein (30). However, redirecting NKTs for the targeting of tumor cells via HLA class I restriction has so far remained unexplored.

Here, we have shown that NKTs expressing an ectopic HLA class I–restricted TCR can be generated in less than 3 weeks of culture, and in sufficient numbers for the clinical translation. We showed that the ectopic TCR can displace the iTCR on a proportion of NKTs by outcompeting for binding to the CD3 complex. This phenomenon occurred when the mRNA of the ectopic TCR chains was overexpressed compared with the endogenous iTCR, with higher transcript numbers dictating which receptor was expressed on the cell surface of NKTs. Interestingly, Sommermeyer and colleagues previously showed that a transgenic TCR can outcompete the endogenous TCR in CMV-specific T-cell clones (31). Our study, thus, underlines that the restricted TCR repertoire of

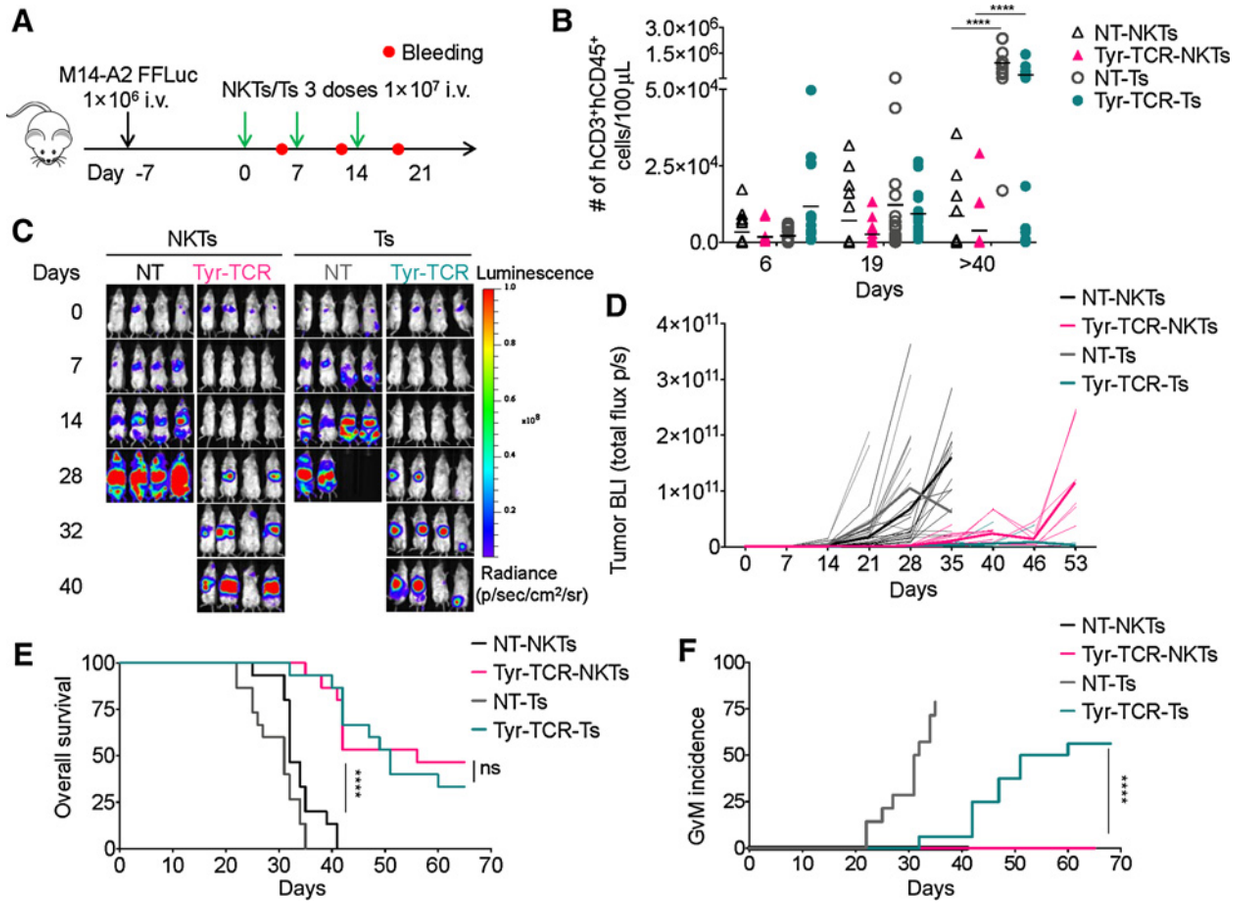

Figure 7.

Multiple infusions of Tyr-TCR NKTs control tumor growth without inducing graft-versus-mouse effects. **A,** Schema of the xenograft tumor model in NSG mice inoculated i.v. with M14 cells and treated with 3 injections of NKTs or T cells (1×10^7 cells each). **B,** Quantification of human $CD3^+CD45^+$ cells in the peripheral blood collected 6 to 7 days after each NKT/T-cell infusion and at sacrifice (day > 40; mean shown). ****, $P < 0.0001$, two-way ANOVA with Bonferroni correction. **C** and **D,** Representative tumor BLI (**C**; color scale: min = 4.00×10^6; max = 1.00×10^8) and BLI kinetics (**D**) of all treated mice in four independent experiments engrafted with the eGFP-FFluc–labeled M14-A2 cells and treated with NT-NKTs ($n = 15$), Tyr-TCR NKTs ($n = 15$), NT-Ts ($n = 15$), or Tyr-TCR-Ts ($n = 15$). Dotted lines represent individual mice, and bolded solid lines represent the mean for the group. NT-NKTs versus Tyr-TCR NKTs $P < 0.0001$ at days 28 and 35, two-way ANOVA with Bonferroni correction. Tyr-TCR NKTs versus Tyr-TCR Ts $P < 0.0001$ at day 53, two-way ANOVA with Bonferroni correction. p/sec or p/s, photons/second. **E,** Kaplan–Meier survival curve ($n = 15$ mice/group); ****, $P < 0.0001$, log-rank test. ns, not significant. **F,** Graft-versus-mouse (GvM) incidence curve ($n = 15$ mice/group); ****, $P < 0.0001$, log-rank test.

polyclonal NTKs, compared with the broad TCR repertoire of polyclonal T lymphocytes, overcomes the hurdle of gene editing required in polyclonal T cells to knockdown the endogenous TCRs by granting the displacement of the iTCR.

Independent from the expression of the iTCR, TCR NKTs proved to specifically recognize the peptide/HLA-A2 complex and exhibited a potent antitumor effect against HLA-$A2^+$ tumor cells expressing the targeted antigen. TCR NKTs showed fast killing of the target cells and activation as demonstrated by the production of IFNγ. TCR NKTs maintained their specificity *in vivo* and mediated tumor regression leading to improved overall survival. In particular, TCR NKTs could control tumor metastasis within the liver. It has been reported that murine NKTs can accumulate in the liver of mice bearing hepatocellular carcinomas and inhibit the tumor growth in both primary and metastatic liver models (32). It remains to be demonstrated how human NKTs in NSG mice cause a robust antitumor effect in liver metastases. Our antitumor effects were significant, considering that, because NKTs are well known for orchestrating immune responses by inducing maturation of DCs, activation of T and B cells and transactivation of NK cells (33–35), our model likely underestimated the real potentials of TCR NKTs.

Finally, one further advantage of using NKTs rather than polyclonal T cells for TCR expression lies in the reduced risk of GvHD when both ectopic and native TCRs are retained by transduced cells. Preclinical and clinical evidence suggests that NKTs may act as negative regulators of GvHD, making them relevant in the allogeneic context (36–39). Corroborating these clinical suggestions are previous observations that CAR-engineered human NKTs do not cause graft-versus-mouse—a surrogate of GvHD—in NSG mice (29, 37–40). Here, we showed that TCR NKTs could not only be equally effective as TCR-expressing T cells in controlling tumor growth, but that, unlike T cells, they did not cause graft-versus-mouse in NSG mice. Thus, the manipulations needed for appropriate expression of a transgenic TCR and

abrogation of the endogenous TCR in T cells appear dispensable in NKTs. Overall, we showed that using NKTs as a cell platform for TCR expression in cancer immunotherapy is feasible and provide significant advantages compared with T cells. Based on our current analysis, the only requirement for effective antitumor activity via HLA-restricted TCR by NKTs is the need for expressing TCRs characterized by high functional avidity.

Disclosure of Potential Conflicts of Interest

L.S. Metelitsa reports receiving a commercial research grant from and has ownership interest (including patents) in Cell Medica. G. Dotti reports receiving a commercial research grant from Cell Medica and is a consultant/advisory board member for MolMed s.p.a. and Bellicum Pharmaceutical. B. Savoldo reports receiving a commercial research grant from Cell Medica. No potential conflicts of interest were disclosed by the other authors.

Authors' Contributions

Conception and design: E. Landoni, G. Dotti, B. Savoldo
Development of methodology: E. Landoni, L.S. Metelitsa, G. Dotti, B. Savoldo
Acquisition of data (provided animals, acquired and managed patients, provided facilities, etc.): E. Landoni, C.C. Smith, G. Fucá, Y. Chen, C. Sun, B. Savoldo
Analysis and interpretation of data (e.g., statistical analysis, biostatistics, computational analysis): E. Landoni, C.C. Smith, G. Fucá, Y. Chen, C. Sun, B.G. Vincent, L.S. Metelitsa, G. Dotti, B. Savoldo
Writing, review, and/or revision of the manuscript: E. Landoni, C.C. Smith, B.G. Vincent, L.S. Metelitsa, G. Dotti
Administrative, technical, or material support (i.e., reporting or organizing data, constructing databases): E. Landoni
Study supervision: G. Dotti, B. Savoldo

Acknowledgments

The imaging core and UNC Flow Cytometry core facilities are supported in part by an NCI cancer core grant, P30-CA016086-40. This work was supported in part by Cell Medica. B. Savoldo is supported in part by R01HL114564, and G. Dotti is supported in part by R01-CA193140.

The costs of publication of this article were defrayed in part by the payment of page charges. This article must therefore be hereby marked *advertisement* in accordance with 18 U.S.C. Section 1734 solely to indicate this fact.

Received February 25, 2019; revised August 27, 2019; accepted November 7, 2019; published first November 12, 2019.

References

1. Dudley ME, Wunderlich JR, Yang JC, Sherry RM, Topalian SL, Restifo NP, et al. Adoptive cell transfer therapy following non-myeloablative but lymphodepleting chemotherapy for the treatment of patients with refractory metastatic melanoma. J Clin Oncol 2005;23:2346–57.
2. Cieri N, Mastaglio S, Oliveira G, Casucci M, Bondanza A, Bonini C. Adoptive immunotherapy with genetically modified lymphocytes in allogeneic stem cell transplantation. Immunol Rev 2014;257:165–80.
3. Morris EC, Stauss HJ. Optimizing T-cell receptor gene therapy for hematologic malignancies. Blood 2016;127:3305–11.
4. Robbins PF, Morgan RA, Feldman SA, Yang JC, Sherry RM, Dudley ME, et al. Tumor regression in patients with metastatic synovial cell sarcoma and melanoma using genetically engineered lymphocytes reactive with NY-ESO-1. J Clin Oncol 2011;29:917–24.
5. Lu YC, Parker LL, Lu T, Zheng Z, Toomey MA, White DE, et al. Treatment of patients with metastatic cancer using a major histocompatibility complex class II-restricted T-cell receptor targeting the cancer germline antigen MAGE-A3. J Clin Oncol 2017;35:3322–9.
6. Ahmadi M, King JW, Xue SA, Voisine C, Holler A, Wright GP, et al. CD3 limits the efficacy of TCR gene therapy in vivo. Blood 2011;118:3528–37.
7. Bendle GM, Linnemann C, Hooijkaas AI, Bies L, de Witte MA, Jorritsma A, et al. Lethal graft-versus-host disease in mouse models of T cell receptor gene therapy. Nat Med 2010;16:565–70.
8. Mastaglio S, Genovese P, Magnani Z, Ruggiero E, Landoni E, Camisa B, et al. NY-ESO-1 TCR single edited stem and central memory T cells to treat multiple myeloma without graft-versus-host disease. Blood 2017;130:606–18.
9. Robbins PF, Li YF, El-Gamil M, Zhao Y, Wargo JA, Zheng Z, et al. Single and dual amino acid substitutions in TCR CDRs can enhance antigen-specific T cell functions. J Immunol 2008;180:6116–31.
10. Cohen CJ, Li YF, El-Gamil M, Robbins PF, Rosenberg SA, Morgan RA. Enhanced antitumor activity of T cells engineered to express T-cell receptors with a second disulfide bond. Cancer Res 2007;67:3898–903.
11. Cohen CJ, Zhao Y, Zheng Z, Rosenberg SA, Morgan RA. Enhanced antitumor activity of murine-human hybrid T-cell receptor (TCR) in human lymphocytes is associated with improved pairing and TCR/CD3 stability. Cancer Res 2006;66:8878–86.
12. Sommermeyer D, Uckert W. Minimal amino acid exchange in human TCR constant regions fosters improved function of TCR gene-modified T cells. J Immunol 2010;184:6223–31.
13. Bunse M, Bendle GM, Linnemann C, Bies L, Schulz S, Schumacher TN, et al. RNAi-mediated TCR knockdown prevents autoimmunity in mice caused by mixed TCR dimers following TCR gene transfer. Mol Ther 2014;22:1983–91.
14. Singh N, Shi J, June CH, Ruella M. Genome-editing technologies in adoptive T cell immunotherapy for cancer. Curr Hematol Malig Rep 2017;12:522–9.
15. Brennan PJ, Brigl M, Brenner MB. Invariant natural killer T cells: an innate activation scheme linked to diverse effector functions. Nat Rev Immunol 2013;13:101–17.
16. Kronenberg M. When less is more: T lymphocyte populations with restricted antigen receptor diversity. J Immunol 2014;193:975–6.
17. Quintarelli C, Dotti G, De Angelis B, Hoyos V, Mims M, Luciano L, et al. Cytotoxic T lymphocytes directed to the preferentially expressed antigen of melanoma (PRAME) target chronic myeloid leukemia. Blood 2008;112:1876–85.
18. Hoyos V, Savoldo B, Quintarelli C, Mahendravada A, Zhang M, Vera J, et al. Engineering CD19-specific T lymphocytes with interleukin-15 and a suicide gene to enhance their anti-lymphoma/leukemia effects and safety. Leukemia 2010;24:1160–70.
19. Frankel TL, Burns WR, Peng PD, Yu Z, Chinnasamy D, Wargo JA, et al. Both CD4 and CD8 T cells mediate equally effective in vivo tumor treatment when engineered with a highly avid TCR targeting tyrosinase. J Immunol 2010;184:5988–98.
20. Rossig C, Bollard CM, Nuchtern JG, Rooney CM, Brenner MK. Epstein-Barr virus-specific human T lymphocytes expressing antitumor chimeric T-cell receptors: potential for improved immunotherapy. Blood 2002;99:2009–16.
21. Arber C, Feng X, Abhyankar H, Romero E, Wu MF, Heslop HE, et al. Survivin-specific T cell receptor targets tumor but not T cells. J Clin Invest 2015;125:157–68.
22. Pule MA, Savoldo B, Myers GD, Rossig C, Russell HV, Dotti G, et al. Virus-specific T cells engineered to coexpress tumor-specific receptors: persistence and antitumor activity in individuals with neuroblastoma. Nat Med 2008;14:1264–70.
23. Xu Y, Zhang M, Ramos CA, Durett A, Liu E, Dakhova O, et al. Closely related T-memory stem cells correlate with in vivo expansion of CAR.CD19-T cells and are preserved by IL-7 and IL-15. Blood 2014;123:3750–9.
24. Savoldo B, Goss J, Liu Z, Huls MH, Doster S, Gee AP, et al. Generation of autologous Epstein-Barr virus-specific cytotoxic T cells for adoptive immunotherapy in solid organ transplant recipients. Transplantation 2001;72:1078–86.
25. Nazarov VI, Pogorelyy MV, Komech EA, Zvyagin IV, Bolotin DA, Shugay M, et al. TCR: an R package for T cell receptor repertoire advanced data analysis. BMC Bioinformatics 2015;16:175.
26. Hiasa A, Hirayama M, Nishikawa H, Kitano S, Nukaya I, Yu SS, et al. Long-term phenotypic, functional and genetic stability of cancer-specific T-cell receptor (TCR) alphabeta genes transduced to CD8+ T cells. Gene Ther 2008;15:695–9.
27. Willemsen RA, Sebestyen Z, Ronteltap C, Berrevoets C, Drexhage J, Debets R. CD8 alpha coreceptor to improve TCR gene transfer to treat melanoma: down-

regulation of tumor-specific production of IL-4, IL-5, and IL-10. J Immunol 2006;177:991–8.
28. Robbins PF, Kassim SH, Tran TL, Crystal JS, Morgan RA, Feldman SA, et al. A pilot trial using lymphocytes genetically engineered with an NY-ESO-1-reactive T-cell receptor: long-term follow-up and correlates with response. Clin Cancer Res 2015;21:1019–27.
29. Heczey A, Liu D, Tian G, Courtney AN, Wei J, Marinova E, et al. Invariant NKT cells with chimeric antigen receptor provide a novel platform for safe and effective cancer immunotherapy. Blood 2014;124:2824–33.
30. Jiang ZM, Luo W, Wen Q, Liu SD, Hao PP, Zhou CY, et al. Development of genetically engineered iNKT cells expressing TCRs specific for the M. tuberculosis 38-kDa antigen. J Transl Med 2015;13:141.
31. Sommermeyer D, Neudorfer J, Weinhold M, Leisegang M, Engels B, Noessner E, et al. Designer T cells by T cell receptor replacement. Eur J Immunol 2006;36: 3052–9.
32. Ma C, Han M, Heinrich B, Fu Q, Zhang Q, Sandhu M, et al. Gut microbiome-mediated bile acid metabolism regulates liver cancer via NKT cells. Science 2018; 360:pii:eaan5931.
33. Fujii S, Shimizu K, Smith C, Bonifaz L, Steinman RM. Activation of natural killer T cells by alpha-galactosylceramide rapidly induces the full maturation of dendritic cells in vivo and thereby acts as an adjuvant for combined CD4 and CD8 T cell immunity to a coadministered protein. J Exp Med 2003;198: 267–79.
34. Hermans IF, Silk JD, Gileadi U, Salio M, Mathew B, Ritter G, et al. NKT cells enhance CD4+ and CD8+ T cell responses to soluble antigen in vivo through direct interaction with dendritic cells. J Immunol 2003;171:5140–7.
35. Barral P, Eckl-Dorna J, Harwood NE, De Santo C, Salio M, Illarionov P, et al. B cell receptor-mediated uptake of CD1d-restricted antigen augments antibody responses by recruiting invariant NKT cell help in vivo. Proc Natl Acad Sci U S A 2008;105:8345–50.
36. Leveson-Gower DB, Olson JA, Sega EI, Luong RH, Baker J, Zeiser R, et al. Low doses of natural killer T cells provide protection from acute graft-versus-host disease via an IL-4-dependent mechanism. Blood 2011;117:3220–9.
37. Du J, Paz K, Thangavelu G, Schneidawind D, Baker J, Flynn R, et al. Invariant natural killer T cells ameliorate murine chronic GVHD by expanding donor regulatory T cells. Blood 2017;129:3121–5.
38. Chaidos A, Patterson S, Szydlo R, Chaudhry MS, Dazzi F, Kanfer E, et al. Graft invariant natural killer T-cell dose predicts risk of acute graft-versus-host disease in allogeneic hematopoietic stem cell transplantation. Blood 2012;119:5030–6.
39. Malard F, Labopin M, Chevallier P, Guillaume T, Duquesne A, Rialland F, et al. Larger number of invariant natural killer T cells in PBSC allografts correlates with improved GVHD-free and progression-free survival. Blood 2016;127: 1828–35.
40. Rotolo A, Caputo VS, Holubova M, Baxan N, Dubois O, Chaudhry MS, et al. Enhanced anti-lymphoma activity of CAR19-iNKT cells underpinned by dual CD19 and CD1d targeting. Cancer Cell 2018;34:596–610.